

Rendering

Sung-eui Yoon
KAIST
November 1, 2017

- Copyright, Sung-eui Yoon, 2017
- This is downloaded from <http://sglab.kaist.ac.kr/~sungeui/render>.

Chapter 17

Appearance Models

Supporting realistic appearance of various materials is one of main goals of physically based rendering. In prior chapters, we discussed some of basic appearance models such as Phong illumination model and rendering equation. In this chapter, we discuss advanced models supporting a larger set of materials.

17.1 Ward BRDF Model

The Ward BRDF model is one of popular BRDF models compactly representing measured BRDFs with reasonably accuracy and supporting anisotropy [WFA⁺05]. Fig. 17.2 shows two rendering results with the model.

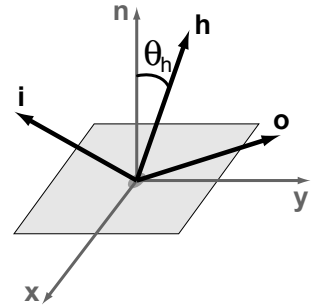


Figure 17.1: Coordinates for the Ward model.

The Ward BRDF model is defined in a 2D plane surface plane (Fig. 17.1), where n is the normal of the surface, and i, o, h are incoming, outgoing, and their halfway directions, respectively.

The Ward BRDF model is defined to have the diffuse term, $\frac{\rho}{\pi}$, and the anisotropic specular term, as the following:

$$f_r(i, o) = \frac{\rho}{\pi} + \frac{\rho_s}{4\pi\alpha_x\alpha_y\sqrt{\cos(i, n)\cos(o, n)}} \exp\left(-\tan^2(h, n) \left(\frac{\cos^2(h, x)}{\alpha_x^2} + \frac{\sin^2(h, x)}{\alpha_y^2}\right)\right), \quad (17.1)$$

where ρ_s indicates the magnitude of the specular lobe, and α_x and α_y represent two magnitudes of anisotropic energy along x and y directions, respectively. Note that the specular term is based on a Gaussian lobe.

The above equation is known to be transformed into the following one, which is more computationally efficient:

$$f_r(i, o) = \frac{\rho}{\pi} + \frac{\rho_s}{4\pi\alpha_x\alpha_y\sqrt{(i \cdot n)(o \cdot n)}} \exp\left(\frac{((h \cdot x)/\alpha_x)^2 + ((h \cdot y)/\alpha_y)^2}{(h \cdot n)^2}\right). \quad (17.2)$$

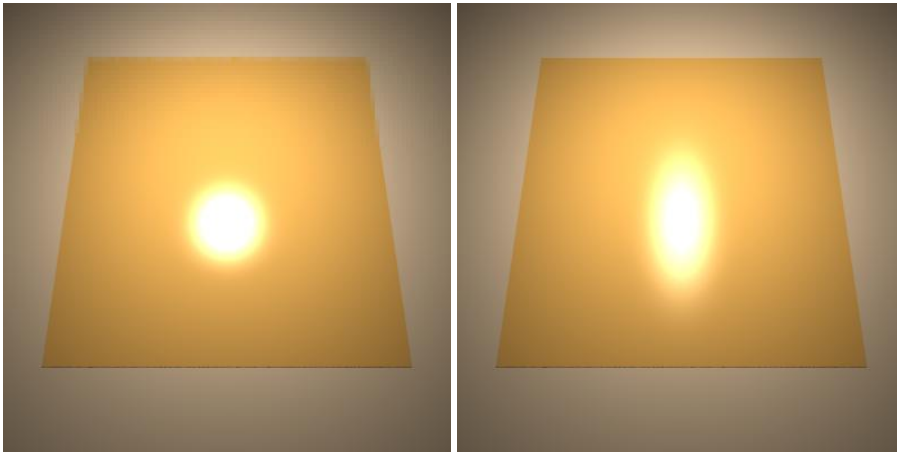


Figure 17.2: These two images show rendering results with the Ward BRDF model. The left is computed with two roughness parameters of 0.1 and 0.1, while the right is with 0.1 and 0.2, resulting in anisotropic glossy effect. These two images are created by S. Premoze.

While the Ward BRDF model supports the anisotropy, it is still an empirical model that does not based on the physical derivation.

17.2 Microfacet Model

The microfacet model is one of most commonly used appearance models that also work well with real surfaces. This model serves as a bidirectional scattering distribution function (BSDF) supporting BRDF, f_r , and BTDF (Bidirectional Transmission Distribution Function), f_t .

When we have smooth surface, reflection and transmission are well represented by the Snell's law (Sec. 10.1). The Snell's law is not enough for rough surface, and thus the microfacet model is proposed to handle such objects with rough surfaces.

The microfacet model considers that real surfaces of objects have microspheres consisting of many small facets, and this detailed microsphere is looked as a simplified macrosphere at a distance (Fig. 17.3). The macrosphere is represented by its normal, n . This model assumes that the microsphere is too small to be seen directly and there is only a single scattering, requiring additional techniques for such small cases that can be seen and multiple scattering; they are discussed in multiple scattering and wave equations [YOON's comment: Fix](#) . Also, the microfacet model assumes that each microsphere works as an ideal reflector, while other reflector types can be used.

The BRDF component of the microfacet model supporting the rough surface is defined as the

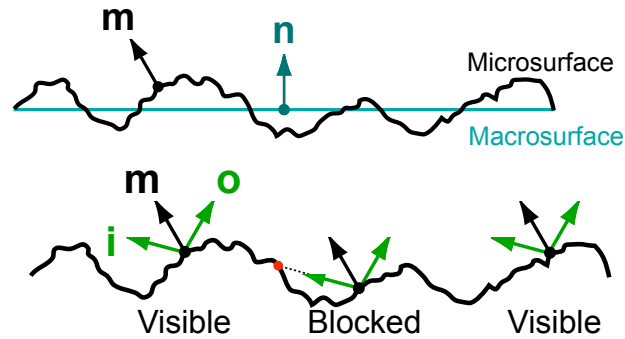


Figure 17.3: Top figure: Detailed microsurface is aggregated as macrosurface at a distant. Bottom figure: some of reflected energy can be blocked by other parts of the surface. Excerpted from [WMLT07]

following:

$$f_r(i, o) = \frac{F(i, m)D(m)G(i, o, m)}{4|i \cdot n||o \cdot n|}, \quad (17.3)$$

where m is the half-way vector and $F(\cdot)$ is the Fresnel term describing how much the incoming light is reflected from each microsurface and thus describes the optical property of the surface. On the other hand, $D(\cdot)$ and $G(\cdot)$ are introduced to explain the geometric shape of the rough surface, and are the microsurface distribution function and shadow-masking function, respectively,

The microsurface distribution function $D(m)$ tells us how much portion of the microsurface heads to the direction of m defined over the solid angle, dw_m . Furthermore, some of them can be invisible due to blocking with other microspheres of the rough surface (Fig. 17.3). We thus use the shadow-masking function $G(\cdot)$.

YOON's comment: Detailed derivation is missing here. I can do that later.

These two functions depend on the geometric shape and are not well defined, but some distributions, e.g., Beckmann and GGX distributions, have been proposed to work reasonably well with measured data. We do not discuss their detailed equations, but their effects on rendering glossy objects are shown in Fig. 17.4.

YOON's comment: multiple scattering:Multiple-Scattering Microfacet BSDFs with the Smith Model

YOON's comment: Discuss diffraction:A Practical Extension to Microfacet Theory for the Modeling of Varying Iridescence



Figure 17.4: The top image row shows a captured image of a metal and its main characteristics, the strong highlight in the center and a smooth falloff. These images are created by Neil Blevins. In the bottom row, from the left, the captured image (highlight) of a chrome, rendered images by GGX, and Beckmann distributions. The GGX has a long tail and thus represents the soft falloff of the highlight. These images are excerpted from [Bur12].



Figure 17.5: They are examples of volumetric materials, clouds and latte, that can be described by radiative transfer equation. The top image is an image shot of a Pixar movie Good Dinosaur, while the bottom one is from Nespresso.

The diagram shows the relationship between differential radiance and its components. On the left, a vector labeled ω points from a point x . This is equated to the sum of four terms: In-scattering (represented by blue lines converging on a point), Out-scattering & absorption (represented by red lines diverging from a point), and Emission (represented by a sun icon). The fourth term is implicitly zero.

$$(\omega \cdot \nabla)L(x, \omega) = \underbrace{\sigma_s(x) \int_{\mathbb{S}^2} f_p(x, \omega_i \rightarrow \omega)L(x, \omega_i) d\omega_i}_{\text{In-scattering}} - \underbrace{\sigma_t(x)L(x, \omega)}_{\text{Out-scattering \& absorption}} + \underbrace{Q(x, \omega)}_{\text{Emission}}$$

Figure 17.6: There are four different interactions between a participating media and the light in a macroscopic manner. They are adopted from slides of Prof. S. Zhao.

17.3 Radiative Transfer Equations

There are many materials that are not simulated well by the rendering equation. Some of them include participating media, e.g., clouds and fog, and translucent materials such as human skins (Fig. 17.5). One may initially want to apply the rendering equation, but the rendering equation is derived based on the assumption that the light energy along a ray does not change. However, they are a kind of volumetric materials wherein the light can scatter and absorb. These effects occur within the material or under the surface of objects, and thus a term of subsurface scattering is also used for referring to the effect. To support this kind of materials, we need a new technique that does not have the assumption.

Radiative transfer [Cha60] is introduced as a mathematical model to explain the interactions of scattering, absorption, and emissions between the participating media and light. Not just in computer graphics, it has been widely used in many different fields including atmospheric science (light transport in the space) and biomedicine (light transport in the human tissue). We now discuss various terms of radiative transfer, but they are empirical models based on our intuitive understanding on the light behavior. While the model is not based on physics theory, it has been proved to be useful in many different fields.

Radiative transfer describes four different events between the light and participating medium in a macroscopic manner. Suppose that we would like to compute the radiance, $L(x, w)$, from a position x to a direction w . Those four events are summarized in below and visualized in Fig. 17.6:

- In-scattering. Light energy from different directions arriving at the location x can scatter to the direction of w , so that the additional light energy is added to $L(x, w)$. The amount

Radiative transfer supports that the light can scatter, absorb, emit in the medium.

of the in-scattering is denoted by $\sigma_s(x)$.

- Out-scattering and absorption. In a similar manner to the in-scattering, the radiance from x to the direction of w can be scattered to other directions and even absorbed within the media. The amount of this factor is known as the extinction factor and denoted as $\sigma_t(x)$.
- Emission. Certain participating media (e.g., fire) can emit light energy, and we thus have the emission term, $Q(x, w)$.

Radiative transfer equation (RTE) mathematically describes these events. For RTE, we start with how the light energy changes differentially, $(w \cdot \nabla)L(x, w)$, from x to the direction w as the following:

$$(w \cdot \nabla)L(x, w) = \sigma_s(x) \int f_p(x, w_i \rightarrow w)L(x, w_i)dw_i - \sigma_t(x)L(x, w) + Q(x, w). \quad (17.4)$$

The first term in the right hand side is the in-scattering term, where $f_p(x, w_i \rightarrow w)$ is a phase function and can be approximated by the angle between two vectors, $f_p(x, (w_i, w))$. An example of the analytic phase function includes the Henyey-Greenstein phase function with a parameter of g :

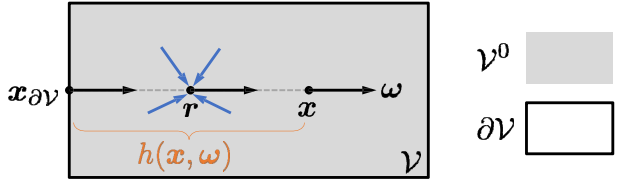
$$f_p^{HG}(\cos \theta, g) = \frac{1}{4\pi} \frac{1 - g^2}{(1 + g^2 - 2g \cos \theta)^{1.5}}, \quad (17.5)$$

where the forward and backward scattering occur mainly at $\theta = 0$ and $\theta = \pi$, respectively, and as g becomes 1, it generates more forward scattering, while g becomes -1 and generates more backward scattering.

Let's look at the second term of Eq. 17.4. It is important to see how the term behaves between two points, say, r and x in the participating media. Let us consider only the term and introduce $T(r \leftrightarrow x)$ as an attenuation term between them, r and x ; i.e., it holds the reciprocity. $T(r \leftrightarrow x)$ is computed as the following:

$$\begin{aligned} (w \cdot \nabla)L(x, w) &= -\sigma_t(x)L(x, w) \Leftrightarrow \\ \frac{(w \cdot \nabla)L(x, w)}{L(x, w)} &= -\sigma_t(x) \Leftrightarrow \\ \int^x \frac{(w \cdot \nabla)L(x', w)}{L(x', w)} dx' &= - \int^x \sigma_t(x') dx' + C \Leftrightarrow \\ \ln L(x, w) &= - \int^x \sigma_t(x') dx' + C \Leftrightarrow \\ L(x, w) &= K \exp \left(- \int^x \sigma_t(x') dx' \right), \end{aligned} \quad (17.6)$$

The attenuation term is derived between two points, to see how much the light is out-scattered and absorbed between them.



$$L(\mathbf{x}, \boldsymbol{\omega}) = \int_0^{h(\mathbf{x}, \boldsymbol{\omega})} \underbrace{T(\mathbf{r} \leftrightarrow \mathbf{x})}_{\text{Attenuation}} \left[\underbrace{\sigma_s(\mathbf{r}) \int_{S^2} f_p(\mathbf{r}, \boldsymbol{\omega}_i \rightarrow \boldsymbol{\omega}) L(\mathbf{r}, \boldsymbol{\omega}_i) d\boldsymbol{\omega}_i}_{\text{In-scattering}} + \underbrace{Q(\mathbf{r}, \boldsymbol{\omega})}_{\text{Emission}} \right] d\tau$$

$$+ \underbrace{T(\mathbf{x}_{\partial V} \leftrightarrow \mathbf{x})}_{\text{Attenuation}} L(\mathbf{x}_{\partial V}, \boldsymbol{\omega}) \quad \text{where } \mathbf{r} := \mathbf{x} - \tau \boldsymbol{\omega}$$

Attenuation Boundary cond.

Figure 17.7: We consider a line represented by $h(x, w)$ from a boundary of the participating volume to the point of x . This figure is adopted from slides of Prof. S. Zhao.

where C, K are constants. When we consider the boundary condition, we get:

$$L(x, w) = \exp\left(-\int_r^x \sigma_t(x') dx'\right) L(x, w),$$

$$= T(r \leftrightarrow x) L(x, w), \quad (17.7)$$

where $T(r \leftrightarrow x)$ is the attenuation term.

In the case of the homogeneous media, we then have $\sigma_t(x) = \sigma_t$, and the attention term $T(r \leftrightarrow x)$ of Eq. 17.7 reduces to $\exp(-||r - x||\sigma_t)$.

Converting to an integral equation. The initial RTE is described by an integro-differential equation involving the integration and differential terms. Since the MC technique works for integral equations, it is better to convert it to an integration form. To do that, we take the integration in the left and right sides. There could be many different integration paths, but we use a line from a boundary of the participating media to the point x along the direction w , i.e., $h(x, w)$ of Fig. 17.7, assuming that it may represent a high energy among many other possible integration paths. Suppose that V and δV indicate the volume of the participating media and its boundary, respectively.

The integro-differential of RTE is transformed into the following integration equation:

$$L(x, w) = \int_0^{h(x, w)} T(r \leftrightarrow x) \left[\sigma_s(\mathbf{r}) \int_{S^2} f_p(\mathbf{r}, \boldsymbol{\omega}_i \rightarrow \boldsymbol{\omega}) L(\mathbf{r}, \boldsymbol{\omega}_i) d\boldsymbol{\omega}_i + Q(\mathbf{r}, \boldsymbol{\omega}) \right] d\tau +$$

$$T(\mathbf{x}_{\delta V} \leftrightarrow \mathbf{x}) L(\mathbf{x}_{\delta V}, w), \quad (17.8)$$

where r is a point in the line from the boundary δV to x , i.e., $r = x - \tau w$. This equation seems complicated, but can be explained intuitively. The last term of the equation represents the radiance at the boundary attenuated to the point x . The first term of the equation considers the same process starting from any point in the line from the boundary to the point x .

Kernel form of RTE. The integral form, Eq. 17.8, of RTE is useful for MC estimation. Nonetheless, it looks a bit complicated. We explain a kernel form of RTE to show its characteristics better. There are various terms of the RTE equation (Eq. 17.8), but some of them are known terms that can be easily computed. Based on this observation, we reformulate the integral form of RTE as the following:

$$L(x, w) = \int_0^{h(x,w)} T(r \leftrightarrow x) \left[\sigma_s(r) \int f_p(r, w_i \rightarrow w) L(r, w) dw_i + Q(r, w) \right] d\tau + T(x_{\delta V} \leftrightarrow x) L(x_{\delta V}, w),$$

$$L(x, w) = \int_0^{h(x,w)} \int T(r \leftrightarrow w) \sigma_s(r) f_p(r, w_i \rightarrow w) L(r, w) dw_i d\tau + \int_0^{h(x,w)} T(r \leftrightarrow w) \sigma_s(r) Q(r, w) d\tau + T(x_{\delta V} \leftrightarrow x) L(x_{\delta V}, w) \quad (17.9)$$

$$L(x, w) = \int_0^{h(x,w)} \int K(r, w_i, x, w) L(r, w_i) dw_i d\tau + S(x, w), \quad (17.10)$$

where a kernel function K is defined to be $T(r \leftrightarrow w) \sigma_s(r) f_p(r, w_i \rightarrow w)$ and a source function S to be $\int_0^{h(x,w)} T(r \leftrightarrow w) \sigma_s(r) Q(r, w) d\tau + T(x_{\delta V} \leftrightarrow x) L(x_{\delta V}, w)$. Since the integration is a linear operator, the above equation can be written in the matrix form. When we use L, K, S to denote matrices of the input radiance, kernel function, and the source function, respectively. The kernel form can be represented by $L = KL + S$, which is similar to the rendering equation.

Solving the radiative transfer equation. Since our radiative transfer equation (Eq. 17.10) is similar to the basic rendering equation (Eq. ?? of Chapter 13), we can use Monte Carlo numerical approaches. A basic approach of computing $L(x, w)$ is to randomly generate τ for computing r (Fig. 17.8) and an incoming direction w_i (Fig. 17.8). We can then recursively apply this approach to compute the incoming direction. **YOON's comment:** We can explain it further by leading to detailed estimators followed by Woodcock tracking.

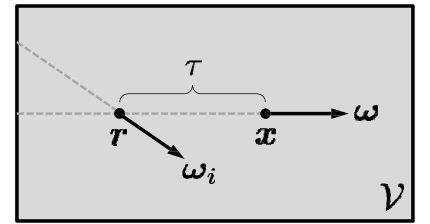


Figure 17.8: Applying the MC method.

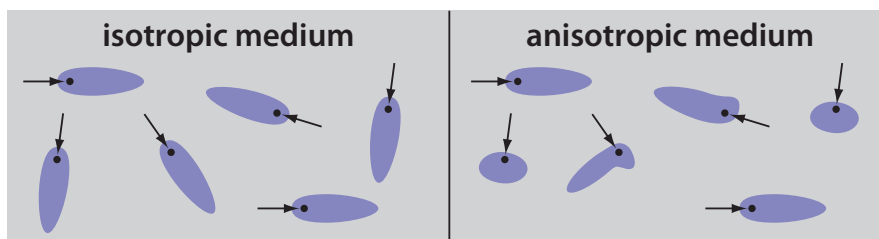


Figure 17.9: Isotropic and anisotropic medium, excerpted from [JAM⁺10].

17.4 Anisotropic Radiative Transfer Equation

RTE explained in Sec. 17.3 supports various types of translucent and participating media. Nonetheless, it is derived under the assumption that underlying particles in the media are isotropic. This assumption works for clouds filled with spherical water droplets and cirrus clouds occurring in high altitude and consisting of randomly oriented ice crystals. For these media, irrespective of incoming light directions, the light energy is scattered in a similar manner.

On the other hand, volumes filled with aligned ice crystals, objects consisting of some types of fibers, e.g., hair, fur, cloths, and woods, and fibrous tissues such as muscles are not well supported. Since there are certain aligned structures in these types of media, the light scatters differently depending on incoming light directions (Fig. 17.9). In this section, we call this anisotropic propagation and discuss how to extend the prior isotropic RTE into anisotropic RTE [JAM⁺10].

The isotropic RTE (Eq. 17.4) is represented as the following:

$$(w \cdot \nabla)L(x, w) = \sigma_s(x) \int f_p(x, (w_i, w))L(x, w_i)dw_i - \sigma_t(x)L(x, w) + Q(x, w).$$

You can see that several terms such as the in-scattering coefficient $\sigma_s(x)$ and the absorption factor $\sigma_t(x)$ that do not depend on the incoming direction of the light. Also, the phase function depends on the angle between w_i and w , not the incoming and outgoing angles. They can be modified to consider the anisotropic propagation and we can have the following anisotropic RTE:

$$(w \cdot \nabla)L(x, w) = \sigma_s(x, w) \int f_p(x, (w_i \rightarrow w))L(x, w_i)dw_i - \sigma_t(x, w)L(x, w) + Q(x, w). \quad (17.11)$$

We now see how we can define these terms depending also on the direction. For this, we also utilize a particle model, since it has been working well for the isotropic case, while various

When there are aligned structures in the medium, we need to consider anisotropic light propagation.

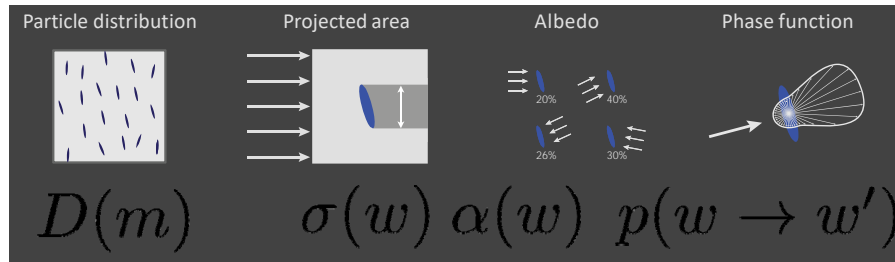


Figure 17.10: These show various factors that describe characteristics of each non-isotropic particle and its distribution, $D(m)$, as a function of a solid angle m . They are adopted from talk slides of [JAM⁺10].

media is not actually based on particles.

Non-spherical particle and its distribution. For the anisotropic RTE, we use a non-spherical particle (Fig. 17.10). For each particle, we use three different characteristic functions of the particle:

1. $\sigma(w)$, the projected area of the particle to the orthogonal direction of w , i.e., w^\perp .
2. $\alpha(w)$, the albedo given the direction w .
3. $p(w \rightarrow w')$, a phase function explaining the energy distribution to w' given w . This is only for the particle, so it is different from the phase function $f_p(\dots)$.

Given an incoming light direction w , $\sigma(w)$ is the proportion of the incoming energy hitting the particle. Given the hit energy, $\alpha(w)$ computes the energy that is scattered, and $p(w \rightarrow w')$ describes how much the scattered energy will head to w' .

We now discuss properties of a volume containing such particles. Two things are introduced for describing the volume:

1. ρ , a density of particles for the volume.
2. $D(m)$, a distribution of particles that are oriented to the direction m .

Based on this distribution $D(m)$, we can expand the prior characteristic functions defined for each particle to its corresponding ones like $\sigma(m, w)$, $\alpha(m, w)$, $p(m, w \rightarrow w')$. Our goal is to derive anisotropic in-scattering function $\sigma_s(x, w)$ and attenuation $\sigma_t(x, w)$ used for the anisotropic RTE (Eq. 17.11). We do not discuss details of deriving these functions here, but discuss how to represent a distributions of non-spherical particles.

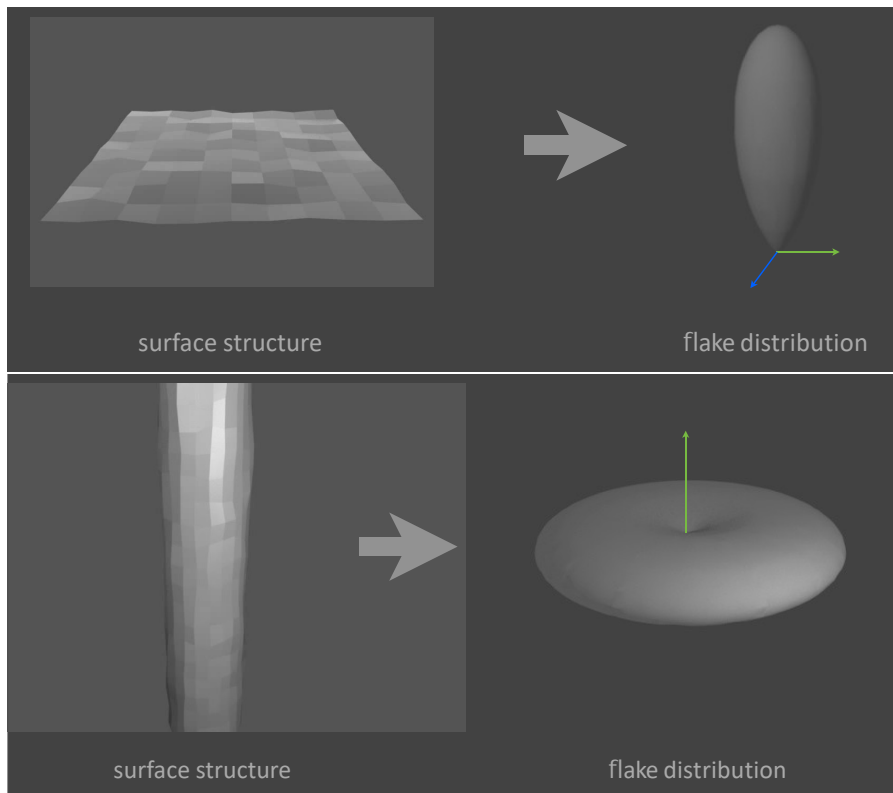


Figure 17.11: These two images show two examples of micro-flake models for two different surface structures. The flake distributions are shown in the polar coordinate. They are adopted from talk slides of [JAM⁺10].

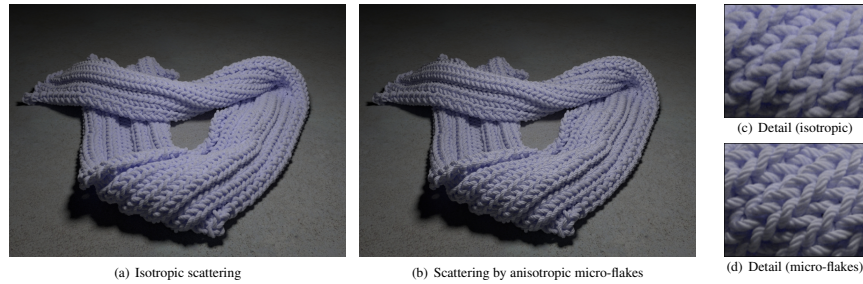


Figure 17.12: These images show rendering results of isotropic and anisotropic RTE. While the isotropic result is rather blurry, the anisotropic approach shows structures of the model better. They are excerpted from [JAM⁺10].

Micro-flake model. To represent the particle distribution of a volume, a micro-flake model is proposed. Fig. 17.11 shows two examples of the micro-flake models for representing rough and fibrous surfaces, respectively. For the case of the planar rough surface, normals of flakes are peaked toward the normal of the rough surface. The micro-flake model is inspired by the micro-facet model, in terms of representing aggregate properties of particles rather than each individual particle or element. A nice property of this micro-flake model is its ability to derive various anisotropic functions such as its phase function in an analytic form, leading to using various numerical solutions of solving the anisotropic equation. Fig. 17.12 shows rendering results of isotropic and anisotropic RTE.